

Coaxial Cable Bragg Grating Sensors for Structural Health Monitoring

Jie Huang¹, Tao Wei¹, Songping Wu², Xinwei Lan¹, Jun Fan², and Hai Xiao¹⁺

Abstract: In situ strain monitoring is critical to ensure the continued safe and reliable operation of various civil structures, such as dams, bridges, and buildings. In situ strain monitoring is especially important for structures that may experience large strains. In this project, a new coaxial cable Bragg grating (CCBG) is developed as a strain sensor, and the sensor's capacity for large range strain measurement is demonstrated for the first time. The sensor device is comprised of regularly spaced periodic discontinuities along a coaxial cable. The discontinuities are fabricated using a computer numerical controlled (CNC) machine to drill holes in the cable. Each discontinuity generates a weak reflection to the electromagnetic wave propagating inside the cable. Superposition of these weak reflections produces a strong reflection at discrete frequencies that can be explained by the Bragg grating theory. By monitoring the resonant frequency shift of the sensor's reflection or transmission spectra, strain measurement sensitivity of $20\mu\epsilon$ and a dynamic range of $50000\mu\epsilon$ (5%) were demonstrated for axial strain measurements. The experimental results show that the CCBG sensors perform well for the large strain measurement needed in structural health monitoring (SHM).

Key words: Coaxial cable Bragg grating; Large strain sensor; Structural health monitoring.

Introduction

In the past two decades, fiber optic sensors have found many successful applications in structural health monitoring (SHM) due to their unique advantages, such as compactness, high resolution, and immunity to electromagnetic interference, remote operation, and multiplexing capability [1]. In general, fiber sensors have relatively small dynamic range due to the limited deformability of silica glass. Various strain transfer mechanisms have been investigated to extend the dynamic range of the sensor devices. For example, through a specially-designed sensor package, a high strain resolution of $10\mu\epsilon$ within a large dynamic range ($12,000\mu\epsilon$) has been demonstrated using an extrinsic Fabry-Perot interferometer (EFPI) [2]. However, when embedded into the structure, the signal transmission line (i.e., the optical fiber) can easily break when it is subjected to a large strain (about 1%) and/or a shear force, causing serious challenges for sensor installation and operation. As such, fiber optic sensors have restricted applications in heavy duty or large strain measurement.

The limitation of the fiber optic sensors in terms of strain sensing is mainly due to the platform of the devices, not the sensing concept. Changing the sensing platform to some other waveguiding media that is more robust than the optical fiber might benefit the development of large strain sensor. Coaxial cable is a good candidate. Coaxial cable and optical fiber are two basic forms of cylindrical waveguiding structures that have been widely used in telecommunications for transmitting signals over a long distance [3,

4]. These two types of cables share the same fundamental physics governed by the same electromagnetic (EM) theory, except that the frequencies of the EM waves they support are quite different. In comparison with optical fibers, coaxial cables can survive a large longitudinal strain and are relatively resistant to lateral force and bending. If the concept of FBG can be implemented onto the coaxial cable, the resulting coaxial cable Bragg grating (CCBG) might provide a solution for some challenging issues (e.g. fragility) faced by FBG sensors. The new CCBG platform will have the same attractive attributes as fiber Bragg grating (FBG) and additional unique advantages such as large strain capability, robust enough to survive harsh conditions, and cost effective for the interrogated instrumentation.

Recently, we have successfully reported and proven the feasibility of the CCBG device [5]. In this paper, we report the modeling and sensing mechanism of the CCBG as well as the detailed experimental results for axial strain measurement.

Principle

As shown in Fig. 1, the proposed CCBG is made by inducing air-holes at periodic distances along the coaxial cable. The air-hole perturbs the electromagnetic (EM) waves propagating in the otherwise continuous coaxial transmission line, resulting in a localized characteristic impedance change (air/dielectric discontinuity point) and thus a partial reflection from the impedance discontinuity. Assuming that all the discontinuities are identical,

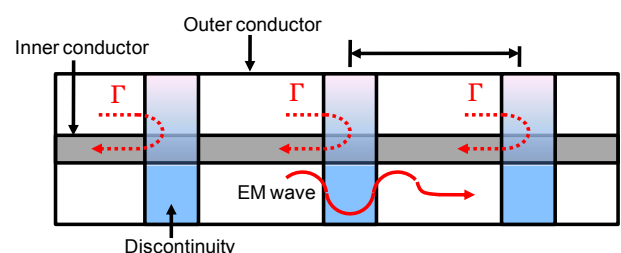


Fig. 1. Schematic Illustration of the Proposed CCBG Device.

¹ Department of Electrical and Computer Engineering, Photonic Technology Laboratory, Missouri University of Science and Technology, Rolla, MO 65409-0030, USA.

² Department of Electrical and Computer Engineering, Electromagnetic Compatibility Laboratory, Missouri University of Science and Technology, Rolla, MO 65409-0030, USA.

⁺ Corresponding Author: E-mail xiaoha@mst.edu

Note: Paper presented at the International Workshop on Smart and Resilient Transportation held April 16-17, 2012 at Virginia Tech, USA; Revised July 27, 2012; Accepted July 30, 2012.

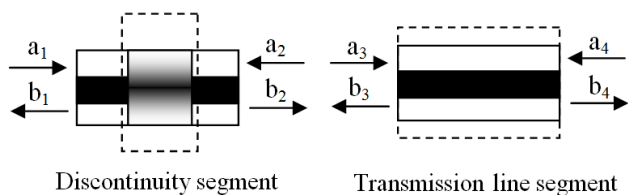


Fig. 2. Segmentation Approach for Transfer Matrix Approximation.

each hole generates a partial reflection with a reflection coefficient Γ along the cable, as shown in Fig. 1. Further assuming that the initial phase at the first hole is zero and the cable is lossless, as the voltage wave travels along the coaxial cable, the accumulated reflection (S_{11}) can be derived by the following equation [6],

$$S_{11} = \frac{1}{V_0} \sum_{n=0}^{N-1} V_r[n] e^{-j2\beta n\Lambda} \quad (1)$$

where V_0 is the input voltage wave, N is the total number of holes on the cable, $V_r[n]$ is the reflected voltage wave at the n th hole, β is the propagation constant of the EM wave travelling inside the coaxial cable, Λ is the period of grating, and $2\beta n\Lambda$ is the phase difference of a wave traveling a round-trip between the first and the n th hole. β can be calculated by $\beta = 2\pi f(LC)^{-1}$ or $\beta = 2\pi f n/c$, where f is the frequency of the EM wave, L and C are the distributed (per unit length) inductance and capacitance of the cable, respectively, n is the refractive index of the inner dielectric material, and c is the speed of light in vacuum.

Assuming a small reflection coefficient of each hole, waves that are reflected more than once carry very little energy so that multiple reflections can be neglected. As a result, the reflection at the n th hole, $V_r[n]$, can be calculated as

$$V_r[n] = V_0 \Gamma (1 + \Gamma)^{2n} \quad (2)$$

where $(1 + \Gamma)$ is the transmission coefficient of the hole. Therefore, the accumulated reflection given in Eq. (2) can be simplified as

$$S_{11} = \frac{\Gamma [1 - (1 + \Gamma)^{2N-2} e^{-2\beta(N-2)\Lambda}]}{1 - (1 + \Gamma)^{2N} e^{-2\beta N\Lambda}} \quad (3)$$

Eq. (3) indicates that the accumulation of the individual reflections eventually results in strong reflections at discrete frequencies where the superposition is in-phase.

Modeling

We propose a two port transfer-matrix method (T-matrix) for numerically simulating the reflection and transmission spectra of the proposed CCBG. Fig. 2 shows a segmentation approach for T-matrix method approximation. The entire cable is divided into multiple discontinuity segments and transmission-line segments, where a_n and b_n ($n = 1, 2, 3 \dots$) are the voltage input and output parameters in each segment, respectively. Each discontinuity segment is investigated using a full-wave numerical solver (Ansoft HFSS) to compute its network parameters, such as S-parameters.

The 2x2 S-matrix of the discontinuity segment and transmission line segment can be written as:

$$\begin{bmatrix} b_1 \\ b_2 \end{bmatrix} = [S_{DS}] \begin{bmatrix} a_1 \\ a_2 \end{bmatrix} = \begin{bmatrix} \Gamma & T \\ T & \Gamma \end{bmatrix} \begin{bmatrix} a_1 \\ a_2 \end{bmatrix} \quad (4)$$

$$\begin{bmatrix} b_3 \\ b_4 \end{bmatrix} = [S_{TS}] \begin{bmatrix} a_3 \\ a_4 \end{bmatrix} = \begin{bmatrix} 0 & e^{(\alpha+j\beta)\Lambda} \\ e^{(\alpha+j\beta)\Lambda} & 0 \end{bmatrix} \begin{bmatrix} a_3 \\ a_4 \end{bmatrix}$$

where $[S_{DS}]$ is the S-matrix of the discontinuity segment, Γ and T are the reflection and transmission coefficients of each dielectric/air discontinuity respectively, $[S_{TS}]$ is the S-matrix of the transmission line segment, Λ is the length of each transmission line segment equaling the period of the grating, α is the transmission loss of the cable, β is the propagation constant, and Γ and T can be numerically simulated by a commercial full-wave solver including magnitude and phase. To make the matrix transfer in a two-port system, the S-matrix must be converted to a T-matrix, which can be mathematically calculated as

$$\begin{bmatrix} b_1 \\ a_1 \end{bmatrix} = [T_{DS}] \begin{bmatrix} a_2 \\ b_2 \end{bmatrix} = \begin{bmatrix} \frac{T^2 - \Gamma^2}{T^2} & \frac{\Gamma}{T} \\ -\frac{\Gamma}{T} & \frac{1}{T} \end{bmatrix} \begin{bmatrix} a_2 \\ b_2 \end{bmatrix} \quad (5)$$

$$\begin{bmatrix} b_3 \\ a_3 \end{bmatrix} = [T_{TS}] \begin{bmatrix} a_4 \\ b_4 \end{bmatrix} = \begin{bmatrix} e^{(\alpha+j\beta)\Lambda} & 0 \\ 0 & e^{(\alpha+j\beta)\Lambda} \end{bmatrix} \begin{bmatrix} a_4 \\ b_4 \end{bmatrix}$$

where $[T_{DS}]$ and $[T_{TS}]$ are the T-matrices of the discontinuity segment and transmission line segment, respectively. From (3), $[a_2, b_2]$ is the input of $[T_{DS}]$, but is also the output of $[T_{TS}]$ ($[b_3, a_3]$). As shown in Fig. 2, the right part of the discontinuity segment a_2 and b_2 are equivalent to the left part of the transmission line segment b_3 and a_3 , respectively. As a result, the T-matrix has the transferring capability along the CCBG to model the device, and the final T-matrix can be written as:

$$\begin{bmatrix} b_1 \\ a_1 \end{bmatrix} = ([T_{DS}] [T_{TS}])^N \begin{bmatrix} a_N \\ b_N \end{bmatrix} = \left(\begin{bmatrix} \frac{T^2 - \Gamma^2}{T^2} e^{(\alpha+j\beta)\Lambda} & \frac{\Gamma}{T} e^{(\alpha-j\beta)\Lambda} \\ -\frac{\Gamma}{T} e^{(\alpha+j\beta)\Lambda} & \frac{1}{T} e^{(\alpha-j\beta)\Lambda} \end{bmatrix} \right)^N \begin{bmatrix} a_N \\ b_N \end{bmatrix} \quad (6)$$

where N is number of segments, or the number of discontinuities of the CCBG. After calculation of the final T-matrix of the CCBG, the last step is to convert the final T-matrix to S-matrix to find the input/output relation.

In the numerical simulation process, $N = 25$, $n = 1.5$ for the dielectric of polyethylene, $\alpha = 0.04$, and $\Lambda = 75$ mm. Fig. 3 plots the calculated reflection and transmission spectra of CCBG. Within the observation bandwidth of 0.1 GHz to 6 GHz, discrete resonances can be found at the fundamental frequency of 1.339 GHz and its harmonics in both reflection and transmission spectra. In this simulated spectrum, the strength of the resonant peaks or dips increased as frequency increased. This can be qualitatively

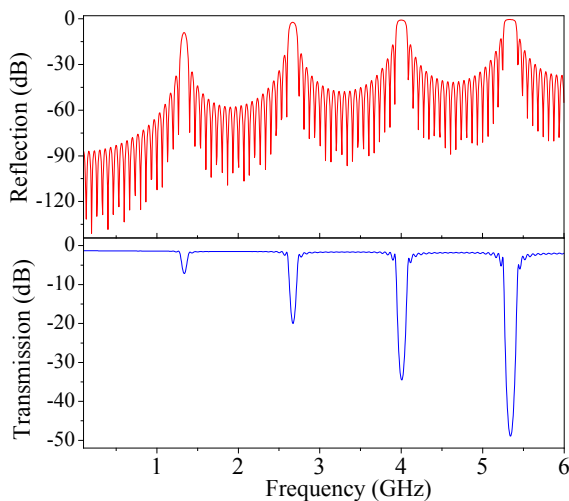


Fig. 3. Calculated Reflection and Transmission Spectra of CCBG by T-matrix Method.

explained by the increasing reflection coefficient (Γ) as a function of frequency numerically simulated by Ansoft HFSS. We also found the quality-factor (Q-factor) of the resonant peaks or dips increased as N increased, which matched well with the FBG theory.

The resonance phenomenon can also be understood by the Bragg grating theory, similar to the well-studied case of FBG, where the forward propagating mode is coupled with the backward propagating mode in the waveguide at discrete frequencies satisfying the following Bragg condition [7],

$$f_{res}^m = \frac{mc}{2n\lambda} = \frac{m}{2\lambda\sqrt{LC}} \quad (7)$$

where L and C represent the inductance and capacitance of the cable, respectively. The resonant frequency is represented as f_{res} , and m is an integer representing the diffraction order of the grating. Using (5) to quickly calculate the parameters in Fig. 3, the resonant frequencies in the simulated spectra match well with the calculation results.

Sensing Mechanism

The applied axial strain in CCBG will induce changes in length (ΔL), inner dielectric radius (Δa) and square root of relative permittivity of the dielectric material ($\Delta\epsilon_r^{1/2}$), which can be expressed as [8],

$$\begin{aligned} \Delta L &= L_S \epsilon \\ \Delta a &= -\nu a \epsilon \end{aligned} \quad (8)$$

$$\Delta\sqrt{\epsilon_r} = -\frac{\epsilon_r^{3/2}}{2} [p_{12} - \nu(p_{11} + p_{12})] \epsilon = -\sqrt{\epsilon_r} P_{eff} \epsilon$$

where L_s is the sensing length of CCBG, ϵ is the applied strain, a is the inner dielectric radius, ν is the Poisson ratio of the dielectric, $\epsilon_r^{1/2}$ is the square root of relative permittivity of the dielectric, p_{11} and p_{12} are the Pockel's coefficients indicating that the relative permittivity of the inner dielectric will be changed (decreased) as stretching the cable, and P_{eff} is the effective coefficient. Considering the EM wave propagating in the inner insulating material, the

changes of dielectrics induced by the axial stress are the only parameters taken into account. Comparing (7) and (8), the changes in L and $\epsilon_r^{1/2}$ are the dominant elements inducing the change in spectra. The change in radius is not taken into account because there only exists a single TEM mode supported by the coaxial cable as the frequency of several GHz ranges.

When an axial strain is applied to the CCBG, a resonant frequency shift will be introduced because of the change of the cable dimension and dielectric constant of the inner dielectric material. The strain induced resonant frequency shift can be expressed as follow,

$$\Delta f = -\frac{L_s}{L_t} \left[\frac{\Delta L}{L_s} - \frac{\Delta\sqrt{\epsilon_r}}{\sqrt{\epsilon_r}} \right] f_{res}^m = -\frac{L_s}{L_t} (1 - P_{eff}) \epsilon f_{res}^m \quad (9)$$

where Δf is the frequency shift of the interrogated resonant frequency induced by the axial strain, and L_t is the total length of the cable under test. It is obvious that the resonant frequency decreases linearly to the applied strain. The reference values of p_{11} , p_{12} , and ν of the polyethylene are 0.337, 0.327, and 0.27, respectively. After a quick calculation, P_{eff} was 0.2216 in this case. The stretch of the cable will increase the length of the cable, but decrease the refractive index of the dielectric. Typically, the length under test will be equal to the length of CCBG, indicating that the strain-frequency slope can be simply written as,

$$\frac{\Delta f}{\mu\epsilon} = -0.78 \times 10^6 f_{res}^m \text{ (Hz / } \mu\epsilon) \quad (10)$$

where the unit of the slope is Hz/ $\mu\epsilon$. Assuming the interrogated resonant frequency is around 3 GHz, the resulted strain-frequency slope will be -2.34 kHz/ $\mu\epsilon$, which matched well with our preliminary result of -3 kHz/ $\mu\epsilon$ in [5].

Fabrication Method

The above investigations into the device physics reveal that the resonance behavior results mainly from the superposition of periodic reflections along the cable axis. The reflections are generated by impedance or refractive index discontinuities as a result of interruption in material properties such as the permittivity and permeability, or in cable parameters such as the resistance, capacitance, or inductance. As such, there are many potential methods to create the impedance discontinuities in a coaxial cable. Here we present a hole-drilling method to create periodic discontinuities along the cable axis.

Hole-drilling on a coaxial cable may degrade the mechanical strength of the cable. On the other hand, the hole-based CCBG sensor might create the opportunity for filling the holes with other types of materials for the purpose of temperature compensation. In addition, the device might be useful for measurement of other parameters such as corrosion and chemical concentration by refilling the holes with various functional materials. Therefore, it deserves a detailed investigation.

Fig. 4 shows the proposed CCBG fabrication system. In order to precisely control the drilling shape, depth, grating period, a computer numerical controlled (CNC) drilling operator (Sherline

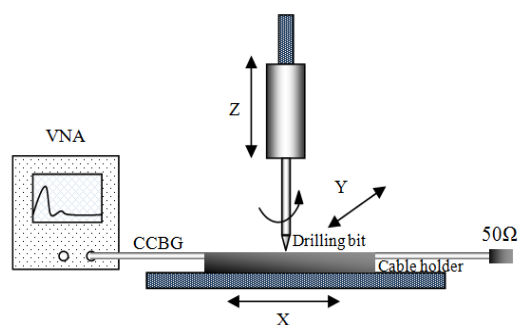


Fig. 4. Proposed CCBG Fabrication System.

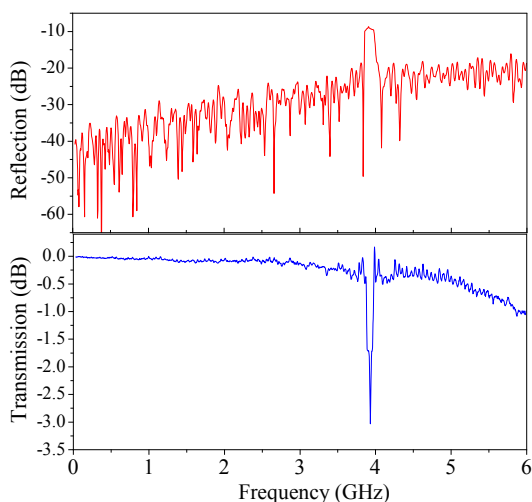


Fig. 5. Reflection and Transmission Spectra of the Fabricated CCBG.

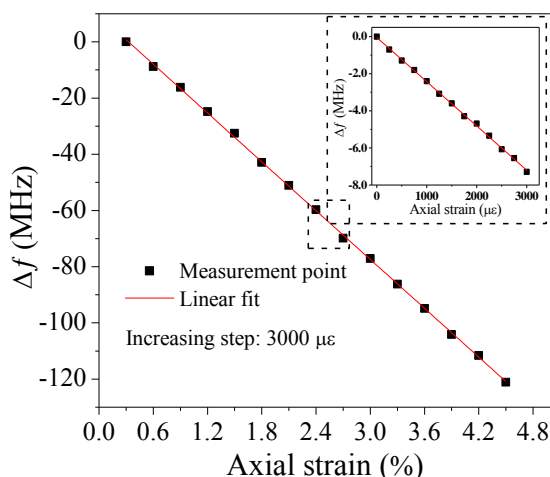


Fig. 6. Resonant Frequency as a Function of Strain: Dynamic Range Test of CCBGs.

P/N 8020A Model 2000) was used, where the minima feeding step of the 3 axes is 100 μm. A vector network analyzer (VNA HP 8753ES) was used to in situ monitor the reflection spectrum during fabrication process. One end of the coaxial cable (50 Ω, Jamco Electronics, RG-58) was launched to the VNA and the other end was matched with a 50 Ω resistance. A 1/12-inch drilling bit was

chosen in this case. All the machines including the VNA were controlled by a computer. The grating period was 25 mm and the number of discontinuities was 41 (in order to make the length of CCBG equaling to 1 m for the convenience of test). The drilling depth was 2.1 mm with the outer diameter of 5 mm of the cable. The coaxial cable was properly calibrated by VNA before fabrication at each time.

Fig. 5 plots the reflection and transmission spectra of a fabricated CCBG. Within the frequency range of 100 kHz to 6 GHz, only one resonant frequency of 3.92 GHz (fundamental frequency) could be found in both reflection and transmission spectra due to the shorter grating period of 25 mm than that of the simulated parameter in Fig. 3. The harmonics are beyond the observation limit of VNA. The resonances shown in the transmission spectrum matched exactly with the reflection spectrum and the experimental results matched well with the simulated results in terms of resonant frequency, strength, and Q-factor. The experimentally measured resonant frequencies also matched well with those calculated by the Bragg condition. The transmission spectrum shows a relatively low transmission loss (≤ 1 dB), indicating that the hole-drilling method did not incur in any extra loss to the cable.

Experimental Results

For the axially tensile strain test, the CCBG of 1 m in length was mounted on a load frame (MTS 880 by TestResources Inc.) using two home machined aluminum clamper and the signals were interrogated by a VNA. The reflection and transmission spectra of the CCBG with and without the clamping fixtures had no evident difference, indicating that the clampers did not introduce noticeable impedance mismatch and reflections. At each increasing step, the transmission and reflection spectra of the device were recorded to find the resonant frequencies. The VNA was configured to acquire the fundamental resonant peak in the reflection spectrum with an observation bandwidth from 3.5 to 4.5 GHz, a total of 1601 sampling points and intermediate frequency bandwidth (IFBW) of 10 kHz.

For the dynamic range test of CCBGs, the load frame elongated the CCBG at a step of 3 mm, corresponding to a strain increasing step of 3000 με, given the initial distance between the two clampers was 1 m. More than 15 loading steps were applied to the CCBG using the load frame until the cable broke. Several CCBGs with the same fabrication parameters were tested. The average breaking point (inner conductor broke first) was around 5%, indicating the dynamic range of CCBG is dramatically greater than 0.4% of the FBG. For each strain point, the reflection and transmission spectra were measured multiple times consecutively, and the averaged spectra were used to find the center frequency of the resonant peaks or dips. Fourth-order polynomial curve-fitting was used to smooth the resonant peak for further improvement of the measurement accuracy.

Fig. 6 plots the change in resonant frequency as a function of the applied tensile strain. In general, the resonant frequency of CCBG decreased almost linearly with a slope of -2.1 kHz/με, which matched well with the calculated slope in (8). The linear strain-frequency shift relation indicates that the CCBG can be used as a sensor for strain measurement after it is properly calibrated. The

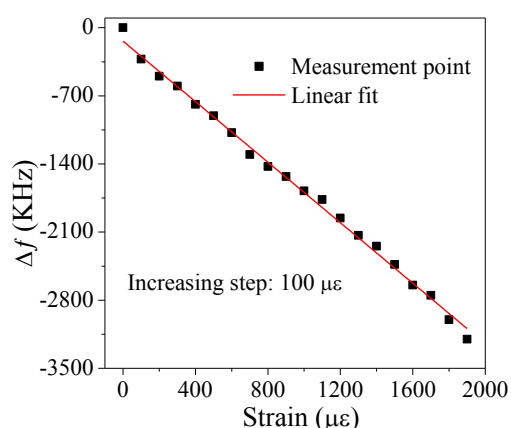


Fig. 7. Resonant Frequency as a Function of Strain: Dynamic Range Test of CCBGs.

dynamic range of 5% indicates the proposed CCBG may provide a solution to the problem issued by FBG in SHM. Interestingly, the Q-factor decreased as the load frame increased. This can be qualitatively explained that the changes in dimension of the cable as the strain increased induced an impedance mismatch to enlarge extra loss for the cable, but the decreasing of Q-factor did not influence the linearity and sensitivity of CCBG. An increasing step of 300 $\mu\epsilon$ was also shown in the inset of Fig. 6. The strain-frequency response was also linear enough.

For the detection limit test of the proposed CCBG, the load frame elongated the CCBG at a step of 0.1 mm, corresponding to a strain increasing step of 100 $\mu\epsilon$. A prestressing load was applied to eliminate the measurement error, and 20 loading steps were applied to the CCBG. The observation bandwidth of VNA was set to 100 MHz around resonant frequency to further enhance the measurement accuracy. The spectra overlapping problem was still severely influencing the signal processing result. And in practical measurements, especially in small increasing step, noise from random reflections along the cable as well as the thermal noise present in the interrogation instruments are unavoidable. To detect the small resonant-frequency shift and achieve high resolution in large strain measurement, a cross-correlation post-processing method was used. The cross-correlation between the two spectra (before and after applying strain) results in a peak whose location provides a direct measure of the resonant-frequency shift. Every point in the spectra will contribute to further enhance the measurement accuracy. Fig. 7 plots the change in resonant frequency as a function of axial strain. With this post-processing method, the strain-frequency response was still linear enough, indicating a high resolution of the proposed CCBG.

Conclusion

To summarize, this paper reports a CCBG as a large strain sensor. The CCBG was fabricated by automatically drilling holes into the coaxial cable at periodic distances along the cable axis. The open hole resulted in an impedance or refractive index discontinuity and partial reflection of the EM wave propagating inside the cable. The

periodic discontinuities produced resonant peaks and dips in reflection and transmission spectra, respectively. These resonances occurred at discrete spectral positions with a fundamental frequency and high order harmonics. No noticeable loss to the EM waves was observed at frequencies other than the resonances. To better understand the physics, the S-parameters of the open hole were calculated using finite element analysis and the device was modeled based on a T-matrix method. The theoretic simulation and experimental result matched well. The experimentally measured resonant frequencies also matched well with those calculated by the Bragg equation. The sensing mechanism has been fully investigated and matched well with the experimental results. When subject to a strain, the resonant frequency of the CCBG device showed a linear response to the loaded strain, indicating the CCBG's potential capability of being used as a strain sensor with a large dynamic range of around 5%. The resolution of CCBG as a strain sensor was 100 $\mu\epsilon$, which also showed a linear response subject to that minima strain after using a cross-correlation post-processing method. The advantages of FBG as a strain sensor were well inherited by the proposed CCBG, and some unique advantages have been explored, indicating CCBG as a strain sensing concept could potentially be effectively applied in SHM.

Acknowledgement

This material is based upon work supported by the National Science Foundation under Grant No. 1100185.

References

1. Li, H.-N., Li, D.-S., and Song, G.-B. (2004). Recent Applications of Fiber Optic Sensors to Health Monitoring in Civil Engineering, *Engineering Structures*, 26, pp. 1647-1657.
2. Bhatia, V., Murphy, K.A., Claus, R.O., Tran, T.A., and Greene, J.A. (1995). Recent Developments in Optical-fiber-based Extrinsic Fabry-Perot Interferometric Strain Sensing Technology, *Smart Materials and Structures*, 4, pp. 246-251.
3. Matick, R.E. (1968). Transmission Line Pulse Transformers-Theory and Applications, *Proceedings of the IEEE*, 56, pp. 47-62.
4. Keiser, G. (2003). Optical Fiber Communications, in *Wiley Encyclopedia of Telecommunications*, ed: John Wiley & Sons, Inc., New York, NY.
5. Wei, T. et al. (2011). Coaxial Cable Bragg Grating, *Applied Physics Letters*, 99, p. 113517.
6. Davidson, D.B. (2005). Computational Electromagnetics for RF and Microwave Engineering - [Book Review], *Aerospace and Electronic Systems Magazine*, IEEE, 20, pp. 27-28.
7. Kersey, A.D. et al (1997). Fiber Grating Sensors, *Journal of Lightwave Technology*, 15, pp. 1442-1463.
8. Li, E. (2007). Temperature Compensation of Multimode-interference-based Fiber Devices, *Optics Letters*, 32, pp. 2064-2066.